

RECONSTRUCTION OF THE SOLAR CORONAL MAGNETIC FIELD, FROM ACTIVE REGION TO LARGE SCALE

T. Amari¹, A. Canou¹, F. Delyon¹, J. J. Aly², P. Frey³, F. Alauzet⁴ and SDO/HMI Team⁵

Abstract. The low solar corona is dominated by the magnetic field which is created inside the sun by a dynamo process and then emerges into the atmosphere. This magnetic field plays an important role in most structures and phenomena observed at various wavelengths such as prominences, small and large scale eruptive events, and continuous heating of the plasma, and therefore it is important to understand its three-dimensional properties in order to elaborate efficient theoretical models. Unfortunately, the magnetic field is difficult to measure locally in the hot and tenuous corona. But this can be done at the level of the cooler and denser photosphere, and several instruments with high resolution vector magnetographs are currently available (THEMIS, Imaging Vector Magnetograph (IVM), the Advanced Stokes Polarimeter (ASP), SOLIS, HINODE, Solar Dynamics Observatory (SDO), or will be shortly available by future telescopes such as EST and solar missions as SOLAR-ORBITER. This has lead solar physicists to develop an approach which consists in "reconstructing" the coronal magnetic field from boundary data given on the photosphere. We will discuss some of the issues encountered in solving this problem as well our recent progress and results at the scale of active region scales or the larger one such as full sun scale.

Keywords: solar corona

1 Introduction

The problem of the Reconstruction of the solar coronal magnetic field from solar photospheric boundary data, have been a very active topic of research those last years due to the arrival of high resolution and low noise vector magnetographs on ground such as THEMIS, SOLIS or on board of present solar mission such as HINODE, SDO/HMI and future ones such as EST, as well as SOLAR-ORBITER. We are not willing to present a review of all existing methods (see Aly & Amari (2007); Schrijver et al. (2006)) but will just say for the purpose of this Paper, that the main classes methods are optimisation methods (Wiegmann 2004) which use all photospheric data and try to minimize a cost function measuring the difference between the computed transverse field and the measured one, those based on magnetohydrodynamics relaxation methods Valori et al. (2005) and on Grad Rubin based method (Sakurai 1981; Amari et al. 1999; Inhester & Wiegmann 2006; Wheatland 2007). Recently (Amari et al. 2006) presented two methods which attempt to solve the Grad-Rubin Boundary Value Problem (GRBVP), namely XTRAPOL and FEMQ, the first one based on a finite difference approximation and the second one a finite element approximation.

Most of the methods however have addressed the active region scale. With the arrival of SOLIS, and SDO/HMI high resolution, composite vector magnetograms made of several active regions, or embedded in a full disk vector magnetogram of synoptic vector magnetograms become possible. Furthermore vector magnetic fields are also measured on stars at a lower resolution and with different technics, with less accuracy (Donati et al. 2007). This therefore raises the issue of availability of such models at this scale, where the sphericity cannot be negligible. Only very recently extension of reconstruction methods to spherical systems for full sun

¹ CNRS, Centre de Physique Théorique de l'Ecole Polytechnique, F-91128 Palaiseau Cedex, France.amari@cphpt.polytechnique.fr

² AIM - Unité Mixte de Recherche CEA - CNRS - Université Paris VII - UMR n° 7158, Centre d'Études de Saclay, F-91191 Gif sur Yvette Cedex, France

³ Laboratoire Jacques Louis Lions, Université Pierre et Marie Curie, 4, place Jussieu, tour 15-25 (3-17), 75005 Paris

⁴ INRIA - Projet Gamma. Domaine de Voluceau - Rocquencourt - B.P. 105.78153 Le Chesnay Cedex (France)

⁵ Stanford University. HEPL Annex, B210.Stanford, CA 94305-4085 USA

scale have been considered. Principally, the optimization methods have been extended to spherical geometry (Wiegelmann 2007). Moreover, either for full disk or synoptic maps strong constraints on spatial resolution are imposed due to the fact that active regions represents only small fraction on the sun surface and therefore neither uniform nor non uniform structured mesh cannot fit such structures in an optimal way..

In the present paper we recall the principles of method we use, show some of our striking results we have obtained at the active region scale. Then we present the extension of our Grad Rubin well posed method to the system of spherical coordinates as well as its current extension to unstructured tetrahedral mesh including the possibility of adaption. As for our cartesian formulation we favor this approach because it correspond to a well posed boundary value problem.

2 The Equilibrium Reconstruction Problem : Boundary Value Problem

In the model we consider, the corona and the photosphere are represented by a domain Ω which can be either the exterior of a sphere or part of it limited in longitude or latitude, or even actually the half-space $\Omega = \{z > 0\}$ and the plane $\partial\Omega = \{z = 0\}$, respectively. Ω is assumed to be filled up with a low beta slightly resistive and viscous plasma embedded in a magnetic field \mathbf{B} which is taken to be force-free and to decrease sufficiently fast to zero at infinity. Therefore, it does obey the equations

$$\nabla \times \mathbf{B} = \alpha \mathbf{B}, \quad (2.1)$$

$$\nabla \cdot \mathbf{B} = 0. \quad (2.2)$$

It results at once from Eqs. (2.1)-(2.2) that the function α satisfies the constraint

$$\mathbf{B} \cdot \nabla \alpha = 0 \quad (2.3)$$

which merely states that α keeps a constant value along any field line.

The set of equations (2.1)-(2.2) has a mixed elliptic-hyperbolic structure. Basically, it can be decomposed into an elliptic part for \mathbf{B} (at α given), and an hyperbolic one for α (at \mathbf{B} given), associated with Eq. (2.3). To solve for the elliptic part, one should give the normal component B_n of the magnetic field on $\partial\Omega$, while to solve for the hyperbolic one, Eq. (2.3) indicates that the value of α should be given on the part $\partial\Omega^+$ of $\partial\Omega$ where $B_n > 0$, say. This leads us to consider the BVP first introduced by Grad & Rubin (1958). It consists of Eq. (2.1)-(2.3) along with the boundary conditions

$$B_n|_{\partial\Omega} = b_0, \quad (2.4)$$

$$\alpha|_{\partial\Omega^+} = \alpha_0, \quad (2.5)$$

where b_0 and α_0 are two given regular functions, and the asymptotic condition

$$\lim_{|r| \rightarrow \infty} |\mathbf{B}| = 0. \quad (2.6)$$

In the numerical practice, instead of having an unbounded domain we consider the bounded domain Ω_b . Then the asymptotic condition (2.6) is no longer useful and the boundary conditions (2.4)-(2.5) are imposed on the whole $\partial\Omega_b$.

2.1 Principle of the Grad-Rubin method

In the Grad-Rubin method, the BVP above is solved iteratively, with its elliptic and hyperbolic parts being solved successively at each step. More precisely, we look for a sequence $(\mathbf{B}^{(n)}, \alpha^{(n)})$ solution of – BVP-GR hereafter –

$$\mathbf{B}^{(n)} \cdot \nabla \alpha^{(n)} = 0 \quad \text{in} \quad \Omega_b, \quad (2.7)$$

$$\alpha^{(n)}|_{\partial\Omega_b^+} = \alpha_0, \quad (2.8)$$

and

$$\nabla \times \mathbf{B}^{(n+1)} = \alpha^{(n)} \mathbf{B}^{(n)} \quad \text{in} \quad \Omega_b, \quad (2.9)$$

$$\nabla \cdot \mathbf{B}^{(n+1)} = 0 \quad \text{in} \quad \Omega_b, \quad (2.10)$$

$$B_z^{(n+1)}|_{\partial\Omega_b} = b_0. \quad (2.11)$$

The iteration process is initialized by choosing for $\mathbf{B}^{(0)}$ the unique solution of

$$\nabla \times \mathbf{B}^{(0)} = 0 \quad \text{in} \quad \Omega_b, \quad (2.12)$$

$$B_z^{(0)}|_{\partial\Omega_b} = b_0. \quad (2.13)$$

To address the $\text{div } B = 0$ constraint, XTRAPOL uses a vector-potential formulation with a particular gauge defined by $\mathbf{B} = \nabla \times \mathbf{A}$ in Ω_b , with the gauge condition $\nabla \cdot \mathbf{A} = 0$ in Ω_b , and $\nabla_t \cdot \mathbf{A}_t = 0$ on $\partial\Omega_b$, where the subscript t in ξ_t stands for the trace (when it exists) of the tangential component on the boundary of the operator or the field ξ . As noted in Amari et al. (2006), this gauge implies that $\partial_n A_n = 0$ on $\partial\Omega_b$, where $\partial_n f = \hat{n} \cdot \nabla f$.

In the vector potential formulation, the iteration on \mathbf{B} translates into an iteration on \mathbf{A} . $\mathbf{A}^{(n+1)}$ is a vector field belonging to the space $[C^2(\Omega_b) \cup C^1(\partial\Omega_b)]^3$.

The characteristics $(\mathbf{X}; s)$ is a solution of (Amari et al. 2006) $\mathbf{X}' = \mathbf{B}(\mathbf{X})$, with $\mathbf{X}(0) = \mathbf{q}$, for \mathbf{q} given in Ω_b (the prime symbol standing for differentiation with respect to the parameter that runs along the characteristics). Then for any node $\mathbf{q}_h \in \Omega_b$ at which α is defined, one gets α_h as

$$\alpha(\mathbf{q}_h) = \alpha_0(\mathbf{X}_{\partial\Omega_b^+}(\mathbf{q}_h)), \quad (2.14)$$

where $\mathbf{X}_{\partial\Omega_b^+}(\mathbf{q}_h) = \mathbf{X}(\mathbf{q}_h, s_{\partial\Omega_b^+})$ is the intersection of $\{\mathbf{X}(\mathbf{q}; s) : s < 0\}$ with $\partial\Omega_b^+$. Since α_0 is known at nodes that do not in general coincide with $\mathbf{X}_{\partial\Omega_b^+}(\mathbf{q}_h)$, we use an interpolation from its four nearest neighbors. We use a high order Adams-Bashford integration scheme with adaptive step size, which also allows us to capture the ending point of the characteristics defining the limits of the computational box.

One major difference between our Grad-Rubin method and the other methods recalled above, is the fact that those methods uses all the photospheric data as boundary conditions (the three components of the magnetic field), and have therefore to face the ill-posedness of the method, while the Grad-Rubiin method uses α only in one polarity and therefore corresponds to a well posed boundary value problem. However it thus results that the values of α computed in the polarity where it is not imposed, may not match the observed values. Very recently a new approach has been proposed in which the values of α are imposed on the boundary as a weight of the values taken on each polarity. Those are obtained as the solution of an optimization problem such that it minimizes the differences between the computed values and the measured ones in the whole photosphere. This new Grad-Rubin-Optimization-Methods has been shown to give good results with robustness (Amari & Aly 2010).

3 Active Region Scale Scheme

The Grad-Rubin method we have developed above has been successful applied to the modeling of several active regions. In particular it has shown that Twisted Flux Ropes are actually at the origin of several structures observed in the corona using various sources of magnetograms. Using THEMIS we have been able to show for the first time that the emergence of of a twisted flux rope from below the photosphere was associated to a flux rope present in the corona (Canou et al. 2009). Moreover using HINODE, it was possible to show that a Twisted Flux Rope was also at the heart of the magnetic configuration supporting a filament (Canou & Amari 2010) as show on Figure 1.

4 Global and Full Disk Schemes

To face the case of large scale synoptic magnetograms, for which the cartesian geometry used at the active region scale is no longer valid, we have extended the Grad-Rubin Method presented above to the system of spherical coordinates. Such type of magnetograms are now provided by SDO/HMI or SOLIS as shown on Figure 3. Moreover the large amount of data imposes the necessity of developing a numerical which is able to run on massively parallel computers..

The couple of hyperbolic and elliptic BVPs are also valid when Ω_b is a spherical shell comprised between the two spheres $S_0 = \{r = r_0\}$ and $S_1 = \{r = r_1\}$, $\{\mathbf{r} = (x, y, z) \in R^3, r_0 < \|\mathbf{r}\| < r_1\}$, with $r_1 > r_0 > 0$. Moreover compared to the cartesian version, the hyperbolic problem is solved such that for a given point in the domain we use mapping from spherical to cartesian coordinates while going back along the characteristic (Amari et al. 2011a). We have applied successfully our solver to the case of the non linear force free Low and Lou solution (Low & Lou 1991) in spherical geometry as shown on Figure 3.

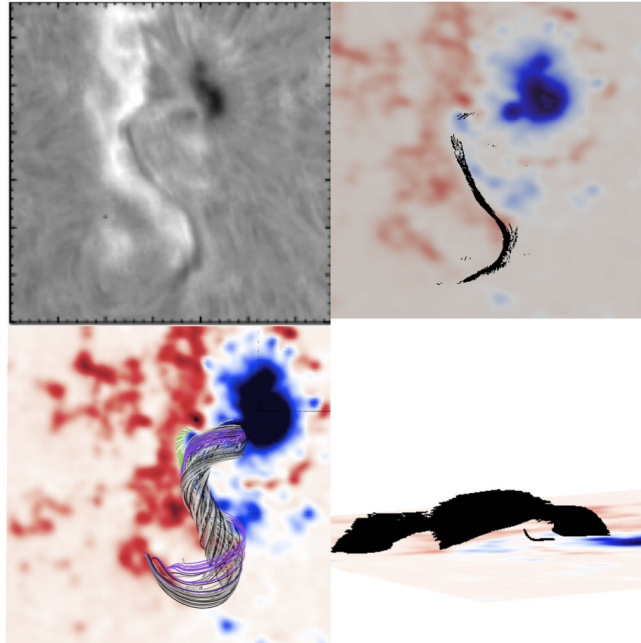


Fig. 1. Comparison of the H- α image taken by SMART (top left panel) on April 29 at 22:10 and the dips corresponding to the non linear force free configuration reconstructed with XTRAPOL (top right panel), in good agreement. A Twisted Flux Rope (bottom left panel) is clearly present and its dips (bottom right panel) exhibit the structure of the observed filament.

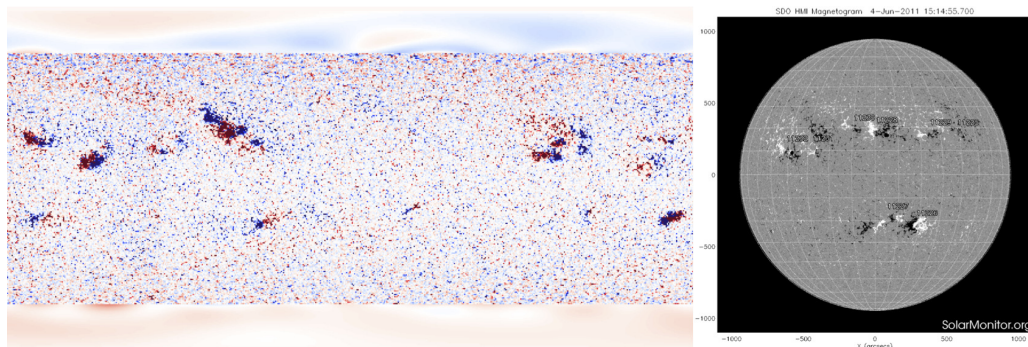


Fig. 2. Example of photospheric magnetic data (photospheric longitudinal field) provided by SDO/HMI for synoptic map (left panel) or full disk (right panel).

The algorithm presented is parallel both for the Elliptic and Hyperbolic problems. We use domain decomposition with the MPI interface on our staggered mesh.

Full disk or synoptic maps impose strong constraints on spatial resolution since active regions represent only a small fraction of the sun surface as shown on Figure 2. Therefore either uniform or non uniform structured mesh cannot fit such structures in an optimal way. For this reason we have recently developed a new approach which consists in extending the Grad-Rubin method to unstructured (tetrahedral) mesh with adaption of the mesh to the solution. This is a quite involving enterprise in which we needed to construct a whole mathematical background including a series of operators such as \mathbf{curl} , $\nabla \cdot$, ∇ on preceding Hilbert Spaces, as well as the boundary value problems on those mesh involving the composition of those operator defined at various locations such as tetrahedra nodes, center, edges, faces (Amari et al. 2011b). We use an adaptation method based on metric computation. Such adaptation can be isotropic or anisotropic. This is used for surface adaptation as well as in the domain during the Grad-Rubin iteration scheme. As seen on Figure 4 this allows to have good surface adaption in the case of synoptic and full disk data. The solution is then computed and the mesh is adapted to the solution in the sense of error targets, in an internal iterative loop during which the solution is

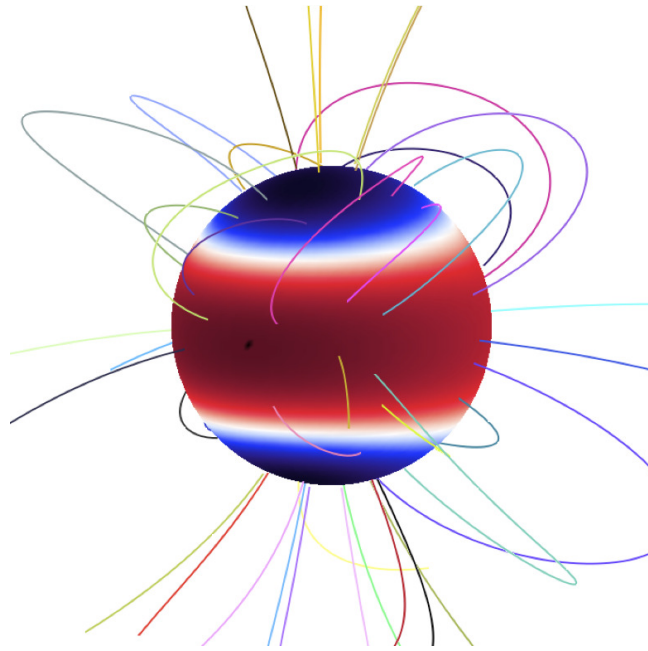


Fig. 3. Field lines of the reconstructed configuration using XTRAPOL in spherical geometry, corresponding to the Low and Lou solution.

computed with the new mesh until adaption is realized. The final solution is obtained in Figure 4 .

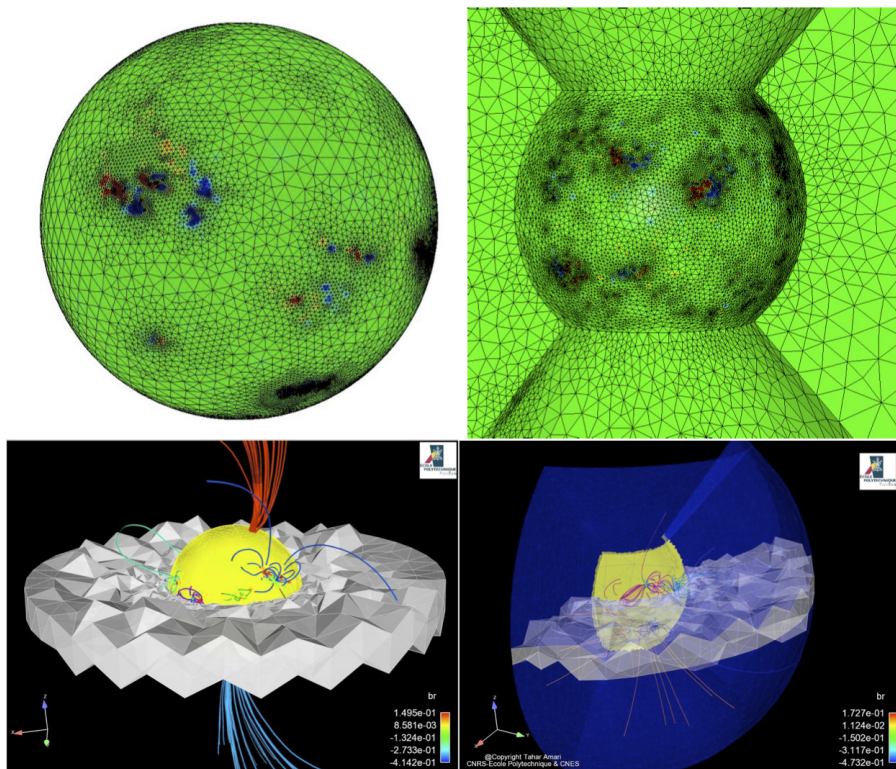


Fig. 4. Resulted mesh obtained after adaption on the photospheric mesh generated after iteration loop for the photospheric synoptic magnetogram (top left panel) and full disk data (right panel). Volume solution and mesh after adaption loop for synoptic case (bottom left panels), and full disk case (bottom right panel).

We acknowledge support from Centre National d'Etudes Spatiales. The numerical simulations performed in this paper have been done on the NEC SX8 supercomputer of the Institute I.D.R.I.S of the Centre National de la Recherche Scientifique.

References

- Aly, J. J. & Amari, T. 2007, *Geophysical and Astrophysical Fluid Dynamics*, 101, 249
- Amari, T. & Aly, J.-J. 2010, *A&A*, 522, A52+
- Amari, T., Aly, J.-J., & Mikic, Z. 2011a, *ApJ*, in press
- Amari, T., Boulmezaoud, T. Z., & Aly, J. J. 2006, *A&A*, 446, 691
- Amari, T., Boulmezaoud, T. Z., & Mikic, Z. 1999, *A&A*, 350, 1051
- Amari, T., Delyon, F., Frey, P., & Aulazet, F. 2011b, *ApJ*, in press
- Canou, A. & Amari, T. 2010, *ApJ*, 715, 1566
- Canou, A., Amari, T., Bommier, V., et al. 2009, *ApJ*, 693, L27
- Donati, J.-F., Jardine, M. M., Gregory, S. G., et al. 2007, *MNRAS*, 380, 1297
- Grad, H. & Rubin, H. 1958, in *Proc. 2nd Intern. Conf. on Peaceful Uses of Atomic Energy*, Vol. 31, United Nations, Geneva, 190–197
- Inhester, B. & Wiegelmann, T. 2006, *Sol. Phys.*, 235, 201
- Low, B. C. & Lou, Y. 1991, *ApJ*, 352, 343
- Sakurai, T. 1981, *Solar Phys.*, 69, 343
- Schrijver, C. J., Derosa, M. L., Metcalf, T. R., et al. 2006, *Sol. Phys.*, 235, 161
- Valori, G., Kliem, B., & Keppens, R. 2005, *Astron. Astrophys.*, 433, 335
- Wheatland, M. 2007, *Solar Phys.*, 245, 251
- Wiegelmann, T. 2004, *Solar Phys.*, 219, 87
- Wiegelmann, T. 2007, *Sol. Phys.*, 240, 227